CHAPTER IV

GROWTH AND CHARACTERISATION OF ORDERED INAS QUANTUM DOTS ON CROSS-HATCH VIRTUAL SUBSTRATE

Self-assembled quantum dots are useful for many electronics and optoelectronic applications such as laser diode, infrared photodetector and superluminescence diode (Song et al., 2004) and light emitting diode (Jo et al., 2005) . Although the benefits of SAQDs cover many applications, their random distributions result in limited usefulness in many electronic and optical devices. Devices such as single electron transistor (Li et al., 2004; Osborn, et al., 2004) and circuits such as quantum cellular automata (Lent et al., 1993; Timler et al., 2002) require uniform QDs. There are various methods which can form laterally- and vertically-ordered QDs. These techniques include several top-down approaches where lithographically-defined substrates, with or without masks, are used as templates for QD growth (Hahn et al., 1998; Liang et al., 2002). They also include several bottom-up approaches where SK growth occurs on pre-existing surface structures such as patterned substrate (Mui et al., 1995), multi-atomic steps (Kitamura et al., 1995), high-index (Nötzel et al., 1996), striped- (Suraprapapich et al., 2005), or superlattice substrates (Mano et al., 2002; Wang et al., 2004) as reviewed in Chapter 3.

One interesting approach is the use of VS where a layer of partially-relaxed layer is used as a template on which more ordered QDs are grown (Zhang et al., 2005; Kim et al., 2004). Epitaxial growth of heterostructures is accompanied by a strain in the epitaxial layer that results from the difference in lattice parameters between the substrate and the epilayer. For large lattice-mismatched systems, 3D islands growth mode are formed after the epilayer thickness is greater then a certain critical thickness. For small lattice-matched systems (<2%), the growth occurs layer-by-layer via a step flow mechanism, and 60° dislocations are nucleated and can thread to the epilayer surface, giving rise to a network of threading which, on the surface, results in non-flat surface morphology. The characteristic undulating surface morphology due to the presence of a network of dislocations is known as a cross hatch.

The formation of cross-hatch patterns has been demonstrated in various material systems such as $In_xGa_{1-x}As/GaAs$ (Rajan et al., 1987), $In_xGa_{1-x}As/InP$ (Dumont et al., 1999) and $Si_{1-x}Ge_x/Si$ (Shiryaev et al., 1997), all are attributed to misfit dislocations and glides. The cross-hatch surface can be used as a template on which subsequent QDs are grown; for examples, for various lattice mismatched systems such as $In_xGa_{1-x}As/GaAs$ (Pan et al., 1998; Leon et al., 2002) and $Si_{1-x}Ge_x/Si$ (Shiryaev et al., 1997). These ordered QDs formed on the VS and their nucleation sites can be controlled by the underlying layer (Hiwatachi and Yamaguchi, 1998; Zhang et al., 2006).

Although the mechanisms of cross-hatch formations have been proposed by several models, their origin remain controversial and unresolved (Andrews et al, 2002). In addition, the understanding of the nature of QDs formation on these substrates is far from complete. The results from this Chapter provide additional information to the nature of QD formation on VS.

The structures of this chapter as follows: the structural characterisation of $In_xGa_{1-x}As$ on GaAs (001) cross-hatch VS is studied in section 4.1 in order to understand the origin of cross-hatch formation. By using the cross-hatch patterns as a starting point, growths of laterally-aligned InAs QDs on these cross-hatch patterns are studied in section 4.2. Three kinds of effects such as growth interruption time, relaxed InGaAs VS and In composition are discussed on the formation QDs on VS. In addition, partial cap of GaAs layer on InAs QDs grown on GaAs layers and VS are performed in order to understand the structural changes of nanostructure during capping process and use a template for further QDs growth.

4.1 Structural Characterisation of InGaAs/GaAs Cross-Hatch Virtual Substrates

A study of cross-hatch pattern for $In_xGa_{1-x}As/GaAs$ single heterostructure is performed. The formation of cross-hatch pattern via generation of MDs is studied by AFM and TEM. In composition in InGaAs layer is confirmed by HRXRD and PL.

For the cross hatch study, 50 nm of $In_{0.15}Ga_{0.85}As$ strained layer is grown on GaAs (001) substrate at T_{sub} 500°C. For the study of surface morphology of cross hatch, T_{sub} is rapidly ramped down to 100°C. The growth rate of InGaAs is 0.06 ML/s and GaAs is 0.34 ML/s.

Figure 4.1 shows the AFM image of the 50 nm-$In_{0.15}Ga_{0.85}As$ layer grown on GaAs (001) substrate. The lattice mismatch between $In_{0.15}Ga_{0.85}As$ and GaAs is 1.07% which is less than 2% where 2D layer-by-layer growth mode is favourable. According to Matthews-Blakeslee's force balanced model, the h_c for the onset of MDs of $In_{0.15}Ga_{0.85}As$/GaAs is 10 nm. The critical thickness for the formation of multiplication dislocation (h_p) is 76 nm (Dunstan et al., 1996). Under the conventional growth of $In_xGa_{1-x}As$ on GaAs, In atoms segregate at the segregation ratio (R) of more than 0.8 (Toyoshima et al., 1993). Therefore, In content in InGaAs layer is reduced because In atoms accumulate at the surface. In order to satisfy the strained layer between h_c and h_p as well as to obtain fair density of dislocation, the thickness of InGaAs layer is chosen as 50 nm for the study of cross-hatch pattern.

Figure 4.1 AFM image of the surface of $In_{0.15}Ga_{0.85}As$ layer on GaAs (001) substrate.

Since the InGaAs strained layer thickness (50 nm) for this sample is significantly larger than the h_c required for MDs (~$10h_c$), the strained layer is partially relaxed by the formation of dislocations at the interface along [1-10] and [110] directions. These dislocations can thread to the surface at 60° angle which results in a cross-hatch appearance aligned along the <110> directions when they are viewed from the top. In other words, the formation of cross-hatch pattern corresponds to the gliding of MD. The correlation between the cross-hatch morphology and the interfacial MD in strained heteroepitaxy has been demonstrated by many research groups. The similar reasons for the formation of cross hatch are claimed by many groups (Chang at al. 1990; Lutz et al. 1995; Yastrubchak at al., 2003). Therefore, the result is in agreement

with the models in which cross-hatch morphology is primarily demonstrated from MD generation and glide processes. However, the result is in contrast to many alternative models for the formations of cross hatch pattern which have been shown by either from composition fluctuations (Glas et al., 1987) or from enhanced growth strained relax regions due to lateral mass transport by surface diffusion (Hus et al., 1992).

In order to investigate the average lateral spacing of the cross hatch, the line profiles of the $In_{0.15}Ga_{0.85}As$ taken across the misfit dislocation lines along the <110> directions indicated by the line marks shown in AFM image of Fig. 4.1 are carried out. The average width and height of the cross-hatch surface undulation taken on the MD lines from the white lines of AFM image in Fig. 4.1 along the [1-10] and [110] directions are different. The average width and height along the [1-10] direction are 840 ± 230 nm and 1.06 ± 0.59 nm whereas along the [110] direction are 505 ± 290 nm and 0.49 ± 0.34 nm respectively. This can be explained in terms of different amplitudes of surface steps along the [110] and [1-10] directions resulting from strain asymmetries in dislocation densities typical for InGaAs/GaAs systems (Kavanagh et al., 1988). The peak-to-valley amplitude of surface undulations along the [1-10] direction is 2.67 nm while those along the [110] direction is 1.42 nm. These two difference values can be explained by a relation between ridges and dislocation which depends on unequal stress on two different sides of the dislocation, which in turn depends on oblique intersection of Burger vectors for 60°-type dislocation. The root-mean-square (rms) roughness of this sample is 0.627 nm.

A lateral periodicity of MDs from AFM result is detected by fast Fourier transform (FFT) analysis. The period (distance) T of signal can be calculated by the relation between period and frequency (f):

$$T\,(\mu m) = 1/f \tag{4.1}$$

Figure 4.2 shows the FFT result obtained from AFM image of Fig. 4.1. From the FFT result, the average frequency of the signal between the original point and the first harmonic signal (fundamental frequency) is 1.123μm^{-1} and thus the period becomes 890 nm according to the equation 4.1. This means that the MDs along [1-10] direction with a lateral spacing of 890 nm are perpendicular to the MDs along [110] direction Therefore, the FFT result is in good agreement with the line profile analysis.

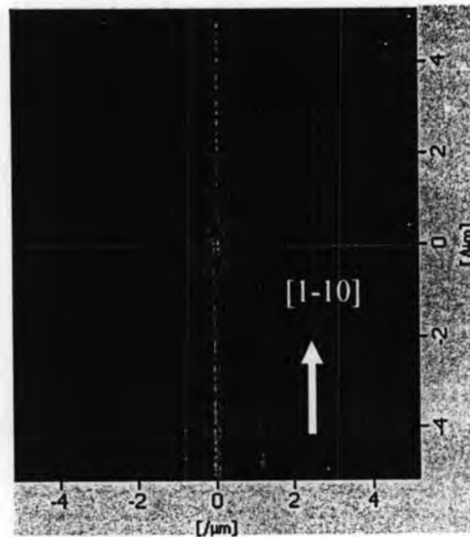

Figure 4.2 FFT analysis of 25×25 μm^2 $In_{0.15}Ga_{0.85}As$ layer on GaAs substrate along [1-10] direction.

Further investigation is carried out by a cross-sectional transmission electron microscopy in order to confirm the origin of cross-hatch pattern. Figure 4.3(a) is the TEM image for the structure in Fig. 4.3(b). A network of dislocations across the InGaAs/GaAs interface due to the misfit strain of heteroepitaxial system can be clearly seen in this figure. Most of the MDs are found to be mixed dislocations that glide on {111} which propagated along <110> directions. This result is in consistent with the result of a surface morphology study which used in AFM measurement. Therefore, the correlation between the cross hatch morphology from AFM image and generation of MDs through the glide process from TEM result can conclude that cross-hatch patterns form after the misfit dislocations are generated.

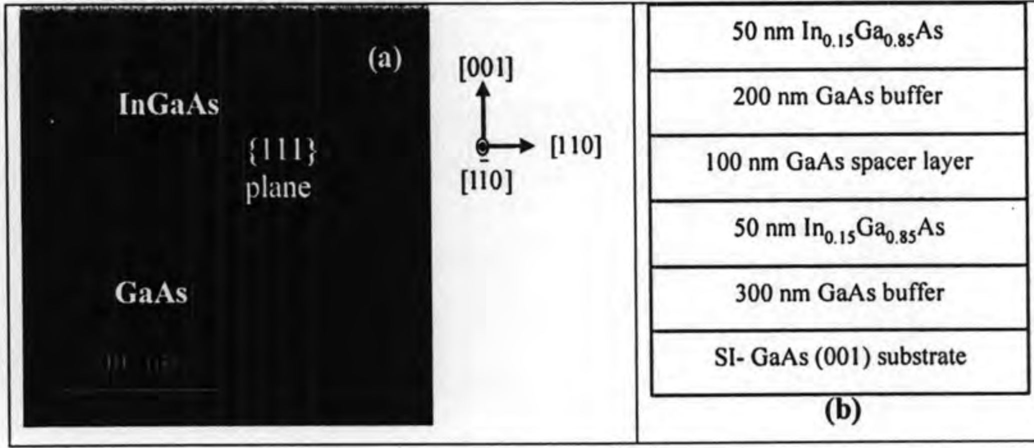

Figure 4.3 (a) Cross-sectional TEM image of $In_{0.15}Ga_{0.85}As/GaAs$ layer and (b) the growth structure.

In order to investigate the crystal quality and the In composition in the InGaAs layer, high resolution X-ray diffraction (HRXRD) measurement is carried out. For all samples, In concentration, x, is estimated from the lattice constant of $In_xGa_{1-x}As$ epilayer (a_e) using Vegard's law:

$$a_e = xa_{InAs} + (1-x)a_{GaAs} \tag{4.2}$$

where a_e, a_{InAs} and a_{GaAs} are the lattice constants of cubic InGaAs, InAs (6.0583 Å) and GaAs (5.6533 Å), respectively. a_e can be determined from the lattice constant in the growth direction of InGaAs epilayer known as out-of-plane lattice constant, $a_\perp$:

$$a_\perp = a_{//} + (a_e - a_{//})(C_{11} + 2C_{12})/C_{11} \tag{4.3}$$

where $a_{//}$ is the in-plane lattice constant of strained InGaAs epilayers, which is equal to a_{GaAs}, C_{11} and C_{12} are the elastic constants for InGaAs. The values of $a_\perp$ and $a_{//}$ are determined from the HRXRD measurements. The entire calculation is repeated three times until the difference between the output and input composition is smaller than error bars by using the linear interpolation of the elastic constants. All the band parameters are used in the equation (4.3) is from the paper of Fan and Yon (2001) (Fan and Yoon, 2001).

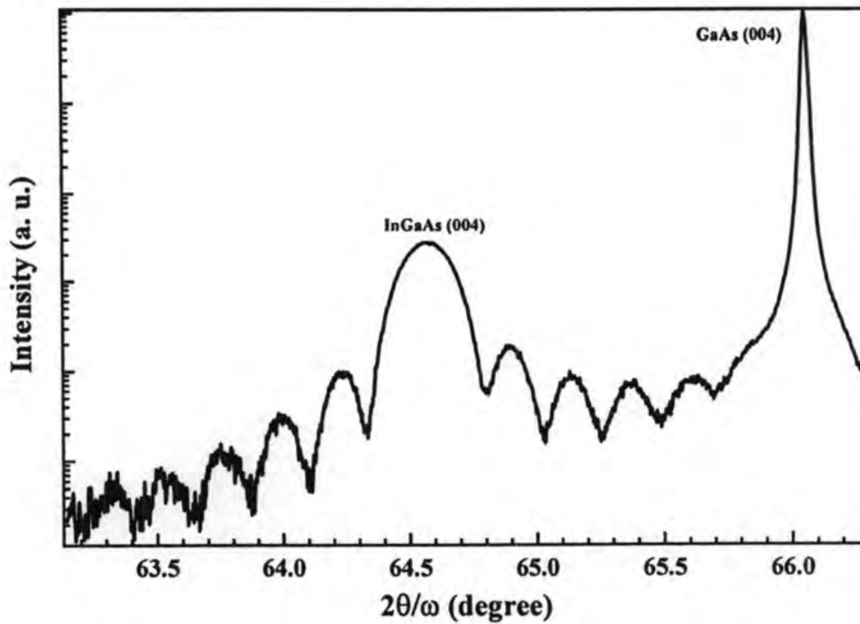

Figure 4.4 HRXRD (004) 2θ/ω spectrum of 50 nm InGaAs layer grown on GaAs (001) substrate.

The (004) HRXRD pattern for the cross-hatch VS $In_{0.15}Ga_{0.85}As/GaAs$ is shown in Fig. 4.4. K_α radiation is used with the wavelength λ=1.540598 Å. There are two distinct peaks in this spectrum. The higher peak corresponds to the (004) plane of GaAs, and the lower one to the (004) plane of InGaAs. Clear Pendellösung fringes (thickness fringe peaks) are also observed. This implies that the alloy composition is homogeneous and the layer has high structural quality with fairly flat interface. The normal lattice constant of the InGaAs layer using equation (4.3) is estimated to be 5.713 Å and In composition is 0.1465.

In order to confirm the In composition, low temperature (77 K) PL measurement was performed. The PL spectrum of $In_{0.15}Ga_{0.85}As/GaAs$ VS is shown in Fig. 4.5. It has three emission peaks. The highest peak at 1.30 eV corresponds to the energy gap of 15% of In composition. The peak at 1.423 eV is related to the exciton peak of GaAs bulk. The wetting layer (WL) peak at 1.37 eV was also observed.

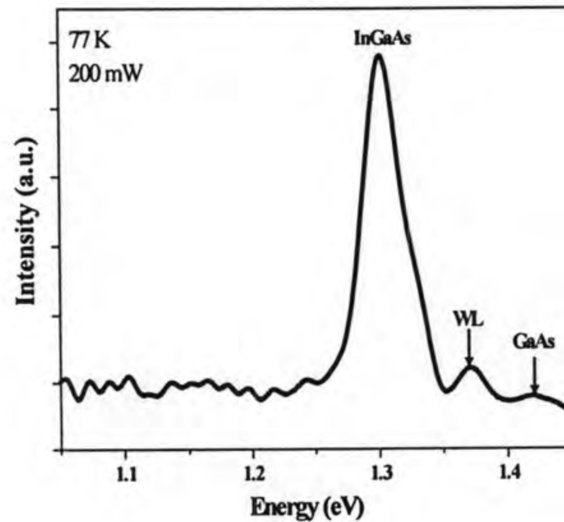

Figure 4.5 Low temperature (77K) photoluminescence spectrum of $In_{0.15}Ga_{0.85}As$ layers grown on GaAs (001) substrate.

In summary, the formation of cross-hatch pattern via generation of MDs and glide process has been explained using AFM and TEM measurements. From the line scan analysis, the width and height of surface undulation along [1-10] is larger than [110] whereas the lateral periodicity of MDs along both directions is the same. FFT analysis has agreed the average lateral spacing of MDs. HRXRD results has proved that crystal quality is rather high and the In composition in InGaAs layer is 15%.

4.2 Growth of InAs Quantum Dots on $In_xGa_{1-x}As$ Cross-Hatch Virtual Substrates

This section presents QDs formation by tuning the growth interruption (GI) time in order to optimize the growth condition of QDs on VS. In addition, the effects of relaxed InGaAs VS on the formation of InAs QDs are studied by growing the various thicknesses of InGaAs strained layers. Finally, In content in InGaAs layers is studied for the better understanding of MD and strain.

4.2.1 Effects of Growth Interruption Time

The growth of long-range QDs on partially-relaxed InGaAs layer with the aid of various GI times is carried out in order to optimize the growth of QDs on cross-hatch VS. Figure 4.6 shows the 0.8 ML of InAs QDs grown on 50-nm $In_{0.15}Ga_{0.85}As$ layer with Fig. 4.6(a) 0 sec, (b) 30 sec and (c) 60 sec GI times respectively. Most of the QDs form on surface ridges along the [1-10] and [110] directions of cross hatch in all figures. However, some of them are randomly distributed on the flat regions which are shown by the white arrows in Fig. 4.6(a). Nevertheless, from the correlation between the positions of QDs in Fig. 4.7(a) and the cross-hatch VS in Fig. 4.7(b), we can conclude that QDs nucleate on *top* of the cross-hatch pattern.

Figure 4.6 AFM images of InAs QDs grown on InGaAs/GaAs with growth interruption times of (a) 0 sec, (b) 30 sec and (c) 60 sec. The height contrast is 8.5 nm.

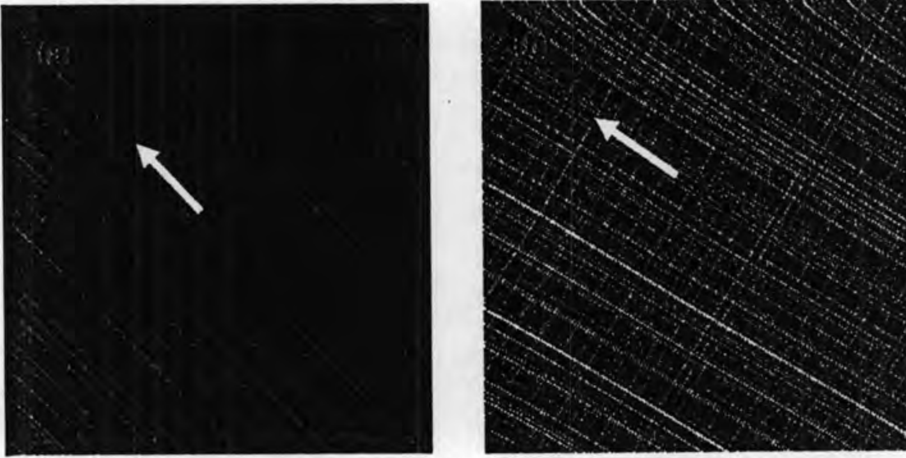

Figure 4.7 AFM images of the (a) surface of $In_{0.15}Ga_{0.85}As$ layer on GaAs (001) substrate and (b) InAs QDs grown on $In_{0.15}Ga_{0.85}As$/GaAs with growth interruption times of 30 sec. All images are 25×25 μm^2 in size and the arrows point towards the [1-10] direction.

A result which differs in one important aspect from those obtained by Zhang et al. (2005) who formed similar VS but obtained QDs along the *side* of the cross-hatch pattern. Zhang et al. introduced 30-sec GI time after the formation of the InGaAs layer and none after QD formation. But in this case, a 2-min GI time is introduced after the formation of the InGaAs layer in order to adjust the In source cell temperature and an additional 30-sec GI time after QD formation for the QD hatches sample shown in Fig. 4.6(b). This gives more detailed growth information of QDs on VS that there is a particular place where the dots prefer to nucleate. The top of the ridges or the cross hatches are where the strain energy is minimum and so In adatoms around the vicinity of the ridges on the surface thus migrate to these energetically favorable locations (Samonji et al., 1999).

Further analyses show that the density and distribution of QDs in each sample are different, although most of the QDs distribute on the cross hatches. Statistical analyses of the AFM images in Fig. 4.6 are shown in Fig. 4.8. From this graph, the total number of QDs across the surface decreases as the GI time increases and the percentages of QDs formed on the cross hatches are 82%, 97% and 66% for samples with GI times of 0 sec, 30 sec, and 60 sec respectively.

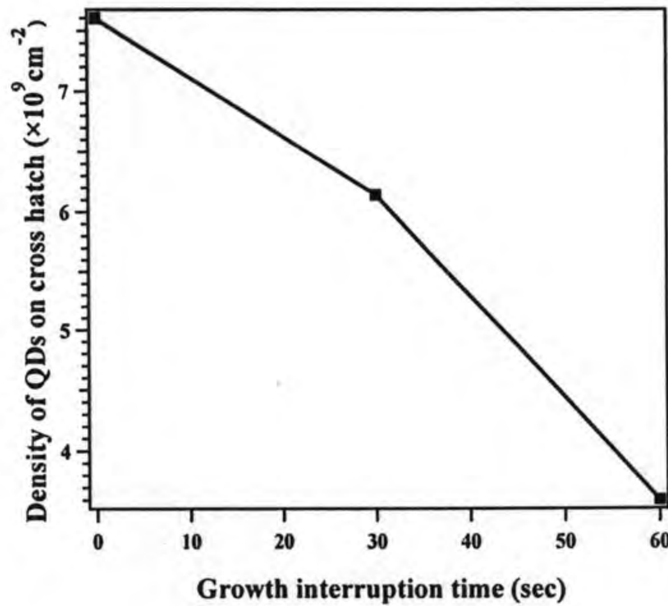

Figure 4.8 Density of QDs on cross hatch with a function of growth interruption time taken from the 3×3 μm^2 by counting the dots along the [1-10] and [110] direction on cross-hatch VS.

In the case of 0-sec GI time, the QDs are "frozen" as soon as they form. And the majority of QDs (82%) are on the cross hatches. In the case of 30-sec GI time, however, surface migration of In adatoms can occur, which for 470°C can be significant. This extra time allows In adatoms to move to the most energetically favourable positions and be incorporated as InAs QDs there. These results in a significant percentage reduction of QDs formed on the flat surface which Fig. 4.6(b) shows that QDs form almost exclusively (97%) on the cross hatches. When GI time allows for 60 sec, not only the QDs are non-uniform but also the positions along the cross hatches are "blurred" and the QD density is reduced by more than 50% from 7.6×10^9 cm^{-2} in Fig. 4.6(a) to 3.6×10^{-9} cm^{-2} in Fig. 4.6(c). The long interruption time affords In atoms more opportunities to desorb from the surface. Therefore, some early-stage QDs in Fig. 4.6(a) disappear completely and the remaining QDs become less homogeneous.

The improved uniformity of QDs as short-duration GI time is introduced has been reported by Kiravittaya et al. (2000) who found that the PL linewidth of QDs decreases after 30-sec GI time. They attributed the linewidth narrowing to the

improvement of QDs size distribution. They also found that the PL linewidth broadens, which implies worsened QD size distribution, for longer GI time (>30 sec) which qualitatively agree with our results.

With the aid of AFM analysis, the dimensions (width and height) of QDs shown in Fig. 4.6(b) on the VS along the [1-10] and [110] directions are measured. The width of QDs is 93 nm and average dot height is (3.20 ± 2) nm in the [1-10] direction. On the other hands, the width of QDs is 75 nm and average dot height is (2.77 ± 2) nm in the [110] direction. These results are attributed to the dimension differences in surface undulations of cross hatches along the [1-10] and [110] directions.

The elongation of QDs can be determined from the size results of QDs. Since the width and height of QDs on VS along [1-10] direction is significantly larger than [110] direction, these results can conclude that the elongation of QDs is in the [1-10] direction. The AFM image of the elongation of QDs in [1-10] direction is shown in Fig. 4.9(a) and the illustration of elongation is shown in Fig. 4.9(b). In order to get the quantitative information, the width of the dots along the <110> direction is measured. Figure 4.10 shows the distribution of the dot width in the [1-10] and [110] directions. The number of counted QDs is 30. From this figure, the average width and height of QDs in the [110] direction is smaller than [1-10] direction. This implies that QDs on cross-hatch VS are elongated in the [1-10] direction.

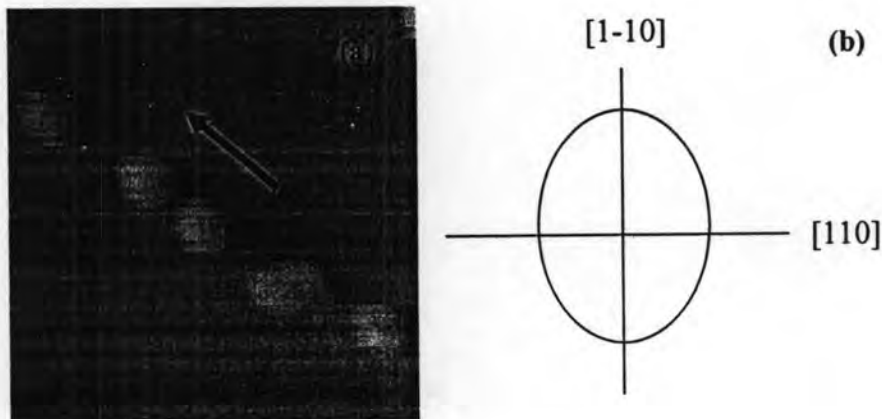

Figure 4.9 (a) AFM image of InAs QDs aligned along [1-10] direction and (b) the orientation of the dots. The arrow indicates [1-10] direction.

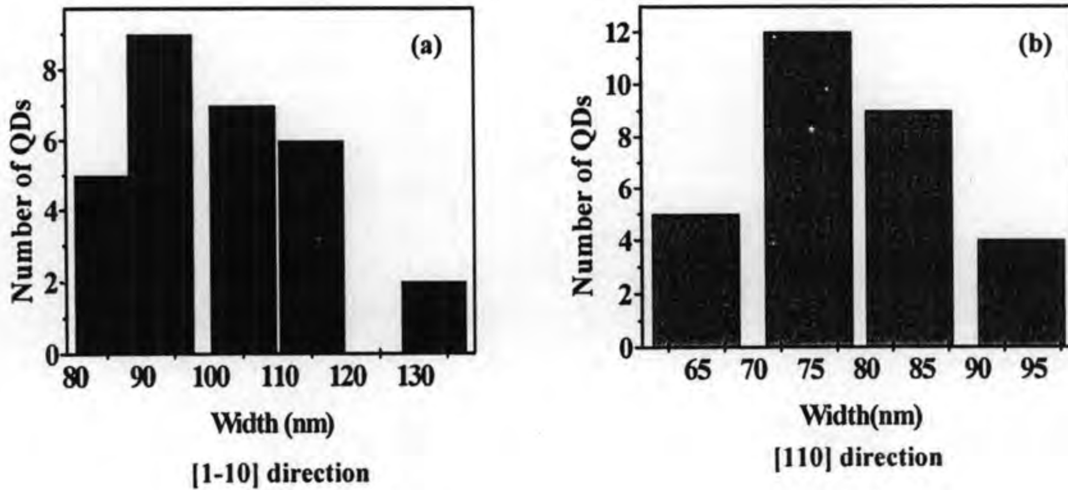

Figure 4.10 Distribution of the width of QDs on VS along the (a) [1-10] and (b) [110] directions.

In summary, formation of QDs on cross-hatch VS has been explained by optimization the growth parameters such as GI time (30 sec) and growth temperature (470°C). The percentage of QDs on top of the surface hatches is enhanced 97% by inserting the 30 sec GI time. Besides, the width and height of QDs on VS along [1-10] is larger than [110] direction due to the asymmetries in dislocation densities which are corresponding to surface undulations of cross hatches.

4.2.2 Effects of Relaxed InGaAs Virtual Substrates

InAs QDs are grown on different relaxed InGaAs VS in order to investigate the effects of VS on the formation of QDs systematically. As discussed in section 4.2.1, 30 sec GI times after the formation of QDs improves the uniformity of QDs. Therefore, all grown samples for QDs on VS are inserted 30 sec GI time under these investigations. InAs QDs grown on 50-nm $In_{0.15}Ga_{0.85}As$ strained layer using GI time 30 sec have resulted in long range and uniform QDs on cross hatch along the <110> direction due to partially strain relaxation of InGaAs layer which gives rise to the formation of cross hatch on the surface. Therefore, the degree of strain relaxation is one of the important parameters for the characterisation of QDs on the VS. In this part, the effect of strain from strained layer is systematically studied by varying the thickness of InGaAs layer from 50 nm to 100 and 150 nm. The surface morphology is

studied by AFM and PL measurement is also performed for the optical investigation of QDs on cross-hatch VS.

Figure 4.11 shows AFM images of (a) and (b) 0.8 ML of InAs QDs on 50-nm and 100-nm InGaAs layers and (c) 0.95 ML of InAs QDs on 150-nm InGaAs layer. The figures show that the surfaces of all samples exhibit a distinct surface undulation along the <110> crystallographic directions, a feature known as cross-hatch pattern. Since the thickness of the InGaAs layer of the three samples under investigation is significantly greater than h_c (i.e. 5, 10 and 15 times h_c), it is expected that the strain energy is partially relaxed through the formation of MDs at the interface.

Figure 4.11 AFM images of InAs QDs grown on $In_{0.15}Ga_{0.85}As$/GaAs virtual substrate where the thickness of the $In_{0.15}Ga_{0.85}As$ layer is (a) 50 nm, (b) 100 nm and (c) 150 nm. The arrows point towards the [1-10] direction.

AFM images in Figs. 4.11(a)-(c) share some similarity and differences. In all figures, the formation of QDs is seen to prefer alignment along two perpendicular directions, [110] and [1-10]. However, the spacing of surface hatches which results in lines of QDs are different. In Fig. 4.11(a), the spacing of surface hatches are separated while partially merged in Fig. 4.11(b) and totally merged in Fig. 4.11(c). The results are attributed to the merging of threading dislocations during the growth of InGaAs layer which results in different surface undulation characteristics. This merging is due to the combination of MDs with increasing thickness of InGaAs layers. In order to confirm the merging of MDs, the line scans taken across the MDs lines along [110]

direction from the 25×25 um^2 AFM images of InAs QDs on VS for three samples is carried out.

The average lateral spacing of cross hatch decreases from 920 nm for 50-nm and 815 nm for 100-nm to 688 nm for 150-nm InGaAs layers respectively. Therefore, the average spacing of cross hatch becomes narrower due to merging of MDs lines during increasing the thickness of InGaAs layers. The results of merging the MDs can be relied even though the line scans are carried out for the samples of VS with grown QDs because the QDs are formed only on the top of the cross-hatch pattern which can see the correlation between the position of QDs and the cross-hatch VS. It means that the position of each formed QD is the place of top of surface undulation and thus the spacing of each QD becomes the separation of each surface undulation along the MDs. Due to merging of MDs, the number of QDs on individual surface ridges in Figs. 4.11(a)-(c) is not the same. The number of QDs per line on the longest cross-hatch pattern along the [110] directions are 50, 65 and 74 dots for the samples with 50-, 100- and 150-nm InGaAs layers.

The line scans taken along the [1-10] direction of the 50-, 100- and 150-nm InGaAs VS samples shown in Figs. 4.11(a)-(c) are correspondingly shown in Figs. 4.12(a)-(c). In each figure, the line scans are taken on the ridges of the cross-hatch pattern itself where QDs are formed. This is shown as the upper lines in Fig. 4.12 apart from Fig. 4.12(b), where line scan for cross-hatch VS without growing QDs on it is performed since any surface ridges are not visible in the AFM image of Fig. 4.11(a). In addition, line scans parallel to the above but shifted slightly to locations with or without minimum number of QDs are also taken and these are shown as the lower lines in Fig. 4.12. The lower line scans represent the surface undulations of the underlying VS. Although the absolute height of the VS does include a thin InAs WL but the change in the surface curvature due to the WL is negligible. From the correlations between the upper and lower scans in Figs. 4.12(a)-(c), the nucleation sites and the degree of groupings of QDs can be concluded. It is clear from the AFM images in Fig. 4.11 that different thicknesses of InGaAs layers give rise to different surface undulations. Although the In composition in all samples is the same (15%), the difference in thicknesses results in differences in strain energy and the subsequent degree of relaxation.

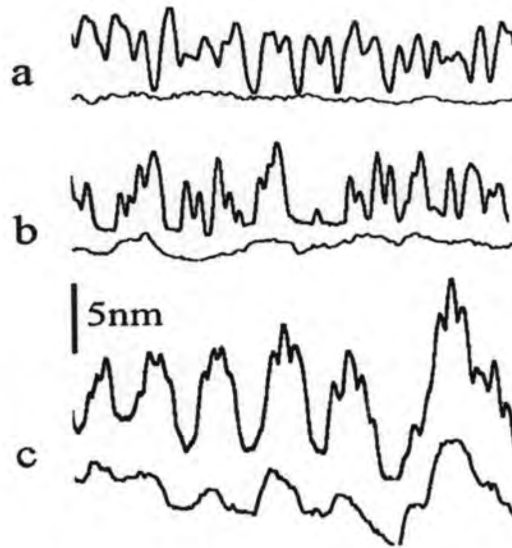

Figure 4.12 Line scans (2.5 μm) along the [1-10] direction taken on a ridge (upper lines) or between ridges (lower) of the cross hatch where InAs QDs are formed on virtual substrates with InGaAs layer thickness of (a) 50-, (b) 100- and (c) 150 nm.

In order to examine the strain relaxation and the crystal quality of the InGaAs/GaAs VS, symmetric (004) and asymmetric (115) HRXRD experiments are performed. Experimental (004) HRXRD patterns of the samples grown on 50, 100 and 150 nm of $In_{0.15}Ga_{0.85}As$ layers is shown in Fig. 4.13(a). It is found that the diffraction angle of (004) InGaAs peak increases as the thickness of the InGaAs layer increases. The narrow measured InGaAs peak shows a clear Pendellösung fringes which indicates that the interface between the substrate (GaAs) and epilayer (InGaAs) is fairly smooth which in turn implies that the density of dislocation generated from the 50-nm InGaAs is lower than the other two samples with 100- and 150-nm InGaAs layers. This reveals that the lattice constant in the growth direction ($a_{\perp}$) of InGaAs decreases as the thickness of the InGaAs layer increases according to Bragg's law which can be examined from the HRXRD results as shown in Fig. 4.13(b). The decrease in $a_{\perp}$ as an increasing of the thickness of InGaAs layer is a clear indication of a higher degree of strain relaxation which are highly dependent on the thickness of the InGaAs underlying layers. A similar result is also observed in the asymmetric (115) XRD patterns shown in Fig. 4.14.

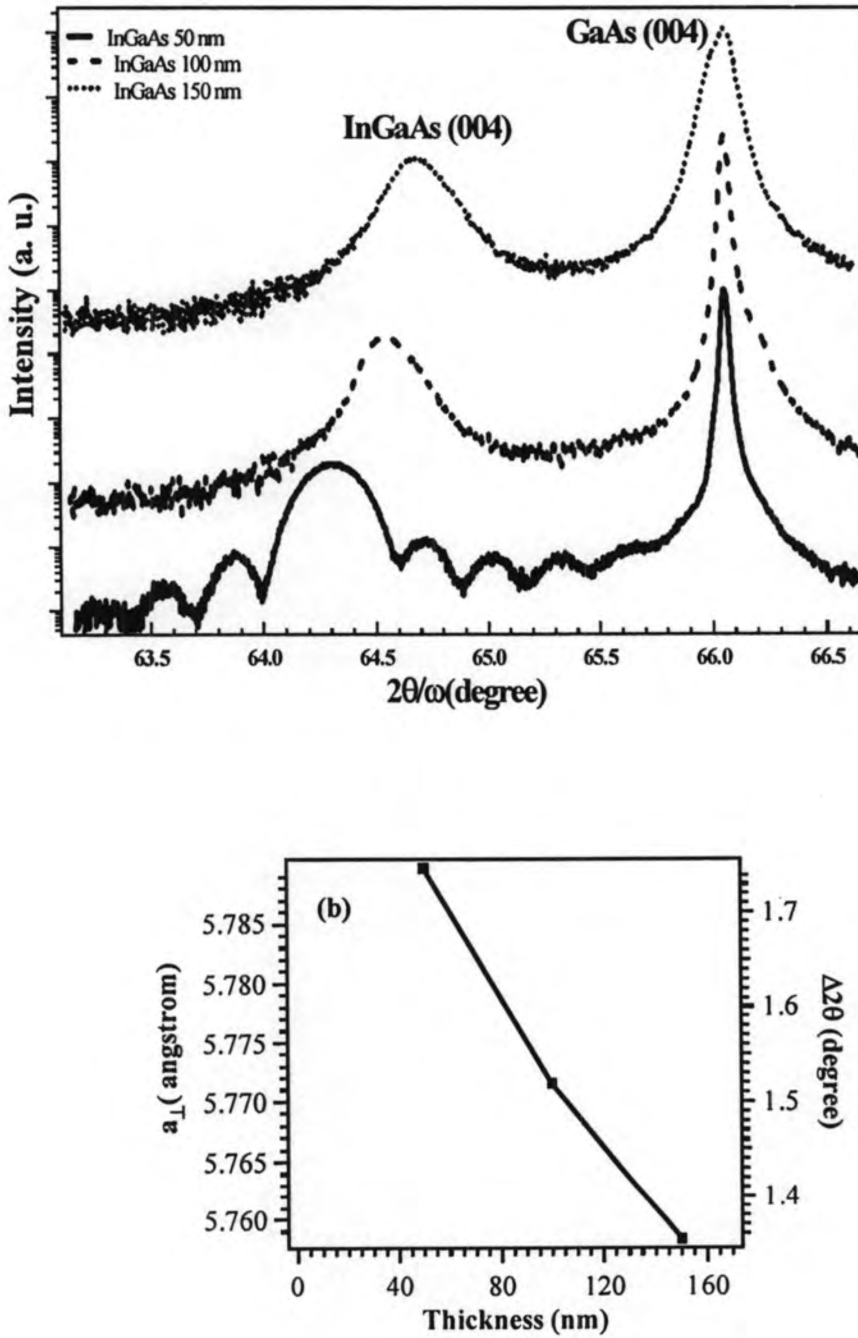

Figure 4.13 (a) HRXRD (004) 2θ/ω curves and (b) the deduced lattice constants ($a_{\perp}$) of the three samples with $In_{0.15}Ga_{0.85}As$ layer thickness of 50-, 100- and 150 nm.

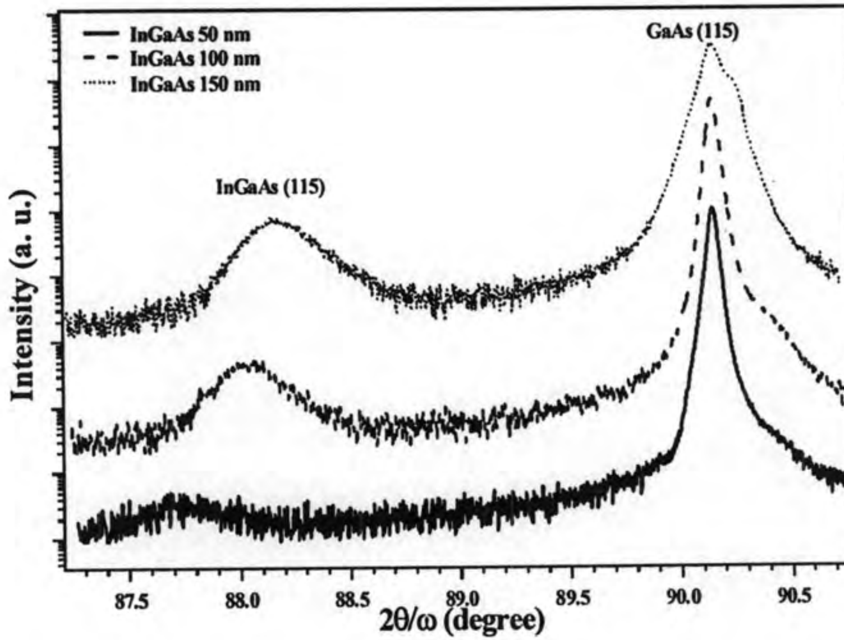

Figure 4.14 HRXRD (115) 2θ/ω curves of the three samples with $In_{0.15}Ga_{0.85}As$ layer thickness of 50-, 100- and 150 nm.

The dependence of strain relaxation in InGaAs layers on these thicknesses are additionally confirmed by calculating percent relaxation from empirical formula (Krishnamoorthy et al., 1992)

$$\% \text{ strain relaxation } \sim 2.0\left(\frac{h-h_c}{h_c}\right) \tag{4.4}$$

for $h_c < h < 30h_c$, where h is the thickness of InGaAs layer, and h_c is the critical thickness for the formation of MDs deduced from Matthews and Blakselee's model. Although InAs QDs are grown on the VS, the strain information of InGaAs layer from HRXRD results can be reliable because the thickness of InAs QDs are only a few monolayer compared to InGaAs strained layers. Therefore, the InAs layer over the InGaAs is not sensitive to investigate the strain relaxation for InGaAs layers. The plot of strain relaxation as a function of thickness based on the calculation is shown in Fig. 4.15. From this figure, the percent relaxation increases as the thickness of the $In_{0.15}Ga_{0.85}As$ layer is increased. For 50-nm $In_{0.15}Ga_{0.85}As$ layer, about 9.6% of the strain from this layer is relieved. 21% and 33% of strains are relieved from the 100- and 150-nm InGaAs layer with the same In content.

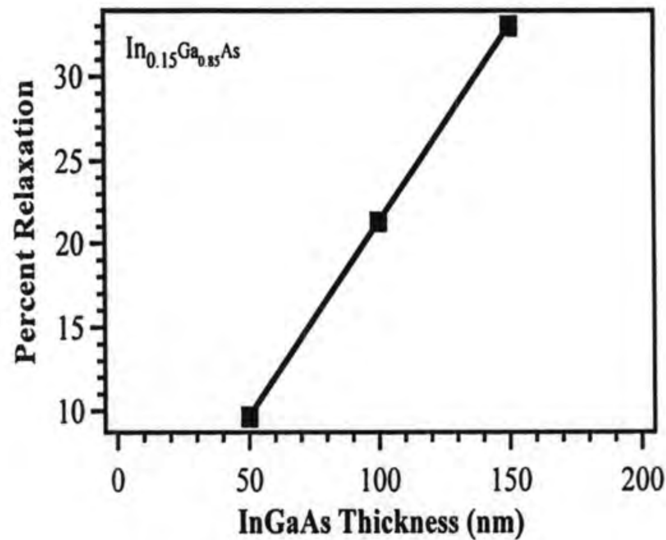

Figure 4.15 A profile showing percent relaxation as a function of $In_{0.15}Ga_{0.85}As$ layers with various thicknesses.

Low temperature (77K) PL measurement is carried out in order to confirm the lattice relaxation observed by HRXRD and optical characterization of the samples. Figure 4.16 shows PL spectrum for the InAs QDs grown on $In_{0.15}Ga_{0.85}As$/GaAs VS with a thickness of 50, 100 and 150 nm. PL emission energies are 1.190, 1.166, and 1.157 eV respectively. PL emission wavelength shows to a clear red shift with increasing the thicknesses of InGaAs layers. In other words, PL peak red shift corresponds to the higher degree of strain relaxation of the InGaAs layers on top of which the QD array is grown. This result may be attributed to the larger QD sizes on the higher degree of strain relaxation VS which can be seen in AFM images in Fig. 4.11. As the strain in the InGaAs layer relaxes more with increasing the thickness of InGaAs layer, PL emission energy thus decreases with increasing degree of strain relaxation. The full width at half maximum (FWHM) is 52 meV for all samples.

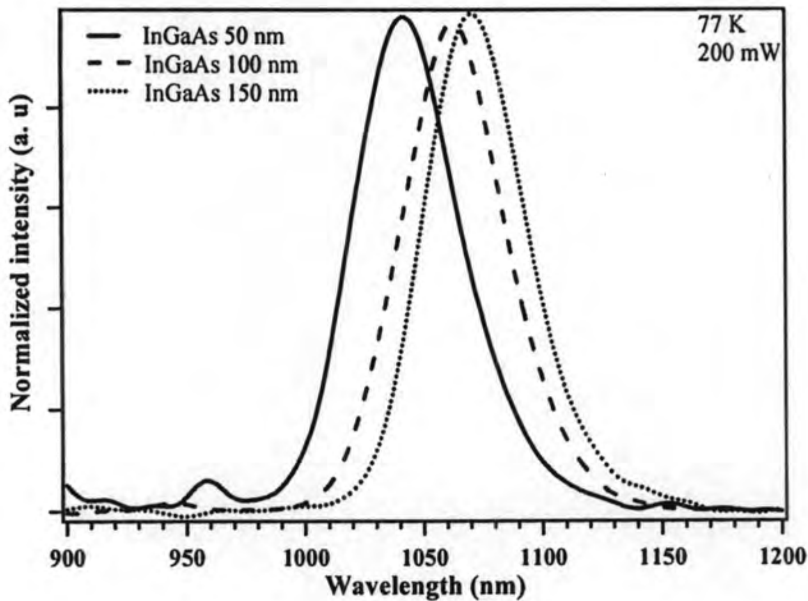

Figure 4.16 Low temperature (77 K) PL spectra of InAs quantum dots grown on partially relaxed $In_{0.15}Ga_{0.85}As$ layers with various thicknesses of 50-, 100- and 150 nm.

Figure 4.17 shows the experimental PL peak emission energy as a function of calculated strain relaxation according to the empirical relation. Emission energy decreases as increasing the percent relaxation. This result is in good agreement with Pan et al. (1998) for the decreasing of PL emission energy with increasing percent relaxation in the $In_{0.15}Ga_{0.85}As$ layer. The XRD results above show that the increased InGaAs thickness results in more strain relaxation and intense surface undulation. These are clearly seen in the line scans as shown in Fig. 4.12 for the samples with the thicker layer of InGaAs.

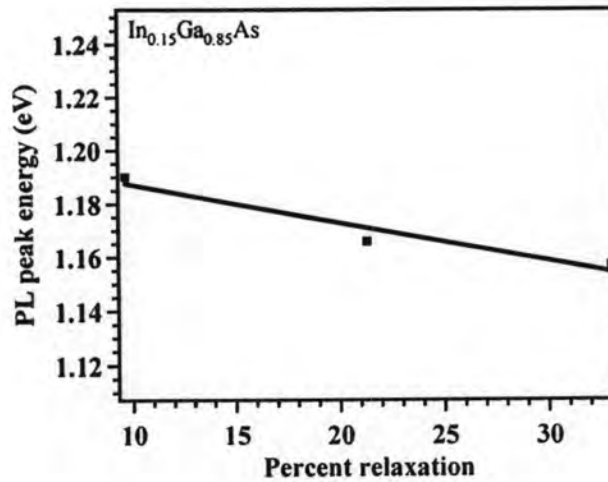

Figure 4.17 Low temperature (77 K) PL emission peak of InAs QDs grown on partially relaxed $In_{0.15}Ga_{0.85}As/GaAs$ VS as a function of calculated percent relaxation of InGaAs strained layers.

In order to illustrate the growth kinetics of this system, we propose an evolution model of InAs QDs on InGaAs VS shown in Fig. 4.18. When the strained layer thickness of InGaAs (50 nm) is comparable to the critical thickness for misfit dislocation, some strain energy is released and generated the misfit dislocations. In this case, since the thickness of InGaAs exceeds by a few times of critical thickness, the misfit dislocations are separated and the grown layer of InAs QDs nucleate on top of the separated cross-hatch pattern as shown in Fig. 4.18(a). This results in QD alignment along the two orthogonal directions as seen in the AFM image in Fig. 4.11(a). These strain energy increases more when the thickness of InGaAs layer increases to 100 nm and give rises to the more strain relaxed area. Correspondingly, some misfit dislocations have the opportunity to merge and so do the surface ridges, giving rise to flat plateaus with wider bases as shown in Fig. 4.18(b) and seen in the AFM image in Fig. 4.11(b). The InGaAs layer in Fig. 4.18(b) is given a lighter shade compared to those in Fig. 4.18(a) to indicate lower strain energy. For a very thick InGaAs layer (150 nm), most misfit dislocations are merged since the strain is almost fully relaxed. The bases of the surface ridges become even wider and QDs now form on these minimum energy sites. Although the size of QDs are relatively uniform (comparing to the as-grown dots), dots that are nucleated in the middle of the ridges

tend to be slightly larger than those at the edges. This is shown in Fig. 4.18(c) and can be seen in the AFM image in Fig. 4.11(c).

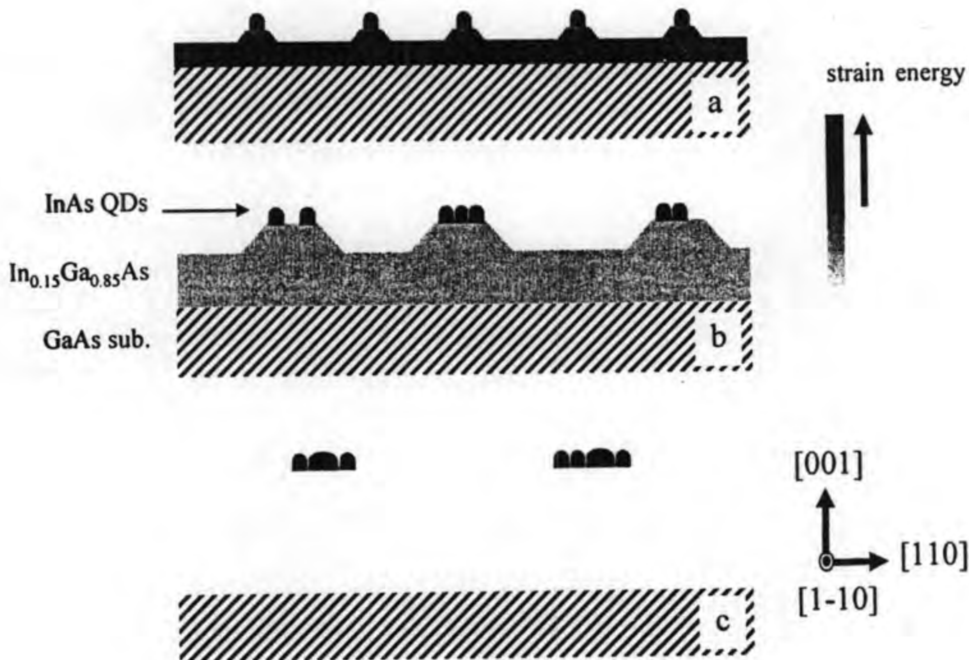

Figure 4.18 Cross-sectional schematic diagram of the evolution of InAs QDs on (a) 50-, (b) 100- and (c) 150-nm InGaAs virtual substrate.

Although the above model describes the evolution of InAs QDs on partially-relaxed InGaAs layer, its qualitative nature is applicable to other material systems with similar non-pseudomorphic growth.

In summary, by growing InAs QDs on relaxed InGaAs virtual substrates, the alignment or spatial correlation of InAs QDs is dictated primarily by the InGaAs layer thickness. The increased InGaAs layer results in a higher degree of strain relaxation as confirmed by (004) HRXRD experiments and the resulting lattice parameters. As the thickness of the InGaAs layer increases, the dislocations have a higher chance of merging and the characteristic surface undulation will change from separated cross hatches to ones with merged hatches. Subsequent growth of InAs QDs on these VS can thus results in QDs which are aligned along two orthogonal directions, as is the case for "thin" InGaAs layer, or grouped into ensembles, as is the case for "thick"

InGaAs layer. Then, an evolution model of InAs QD growth on partially-relaxed InGaAs VS is proposed based on the XRD measurements and AFM images.

4.2.3 Effects of In Composition in $In_xGa_{1-x}As$ Virtual Substrates

InAs QDs grown on $In_xGa_{1-x}As$ VS with different In compositions are studied in order to investigate the effects In composition on InGaAs VS and the formation of QDs. Figure 4.19 shows AFM images of the InAs QDs grown on 50-nm $In_xGa_{1-x}As$ layers with x values of 0.10, 0.13 and 0.15 respectively. The density of MDs along the [1-10] direction changes from 0.8×10^3 lines/cm to 24×10^3 lines/cm by increasing the In composition from 0.10 to 0.15 while those change from 6.8×10^3 lines/cm to 13.2×10^3 lines/cm along the [110] direction. The summary of MDs density along the [1-10] and [110] directions as a function of In composition corresponding to AFM images in Fig. 4.19 is shown in Fig. 4.20. From this figure, the density of cross hatch increases with increasing of In composition. It means that the more InGaAs layer thickness increases, the more InGaAs layer relaxes and the more MDs are generated at the interface between InGaAs layer and GaAs substrate.

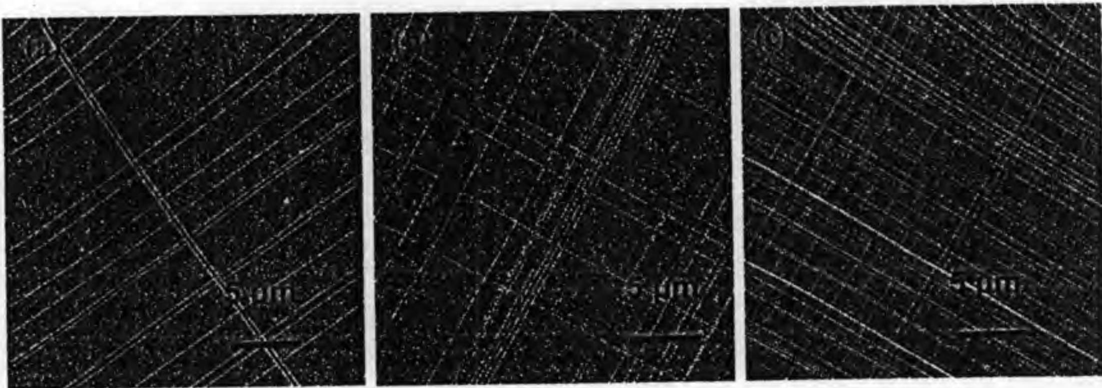

Figure 4.19 25×25 μm^2 AFM images of InAs QDs grown on $In_xGa_{1-x}As$ layers where x is (a) 0.10, (b) 0.13 and (c) 0.15.

Figure 4.21 shows the dependence of density of InAs QDs on the 50-nm $In_xGa_{1-x}As$ cross-hatch VS along the [1-10] and [110] directions with various In compositions extracted from the 3×3 μm^2 area of AFM images in Fig. 4.19. The plot in this figure shows that the density of QDs on VS increases with increasing In

composition because the lattice mismatched between GaAs substrate and InGaAs strained layer increases from 0.72% to 1.07% and thus InGaAs layers relax more and generate more misfit dislocations at the interface and result in more QDs on these misfit dislocations.

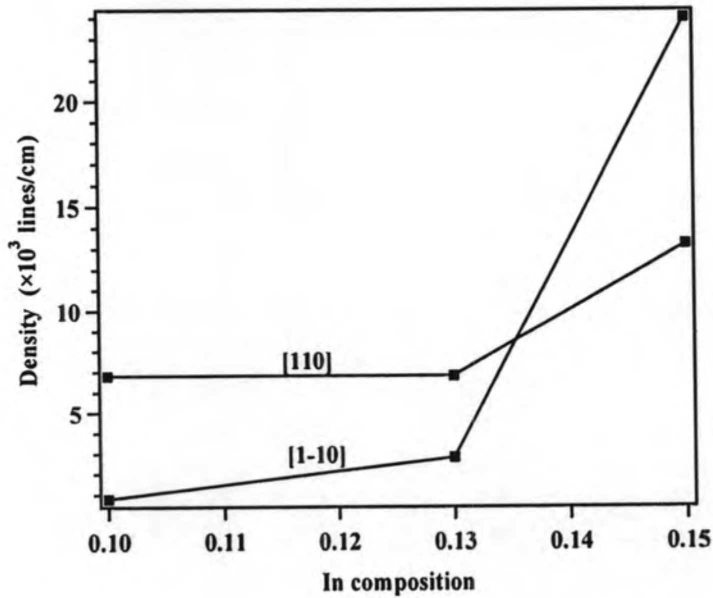

Figure 4.20 The density of cross hatch as a function of In composition.

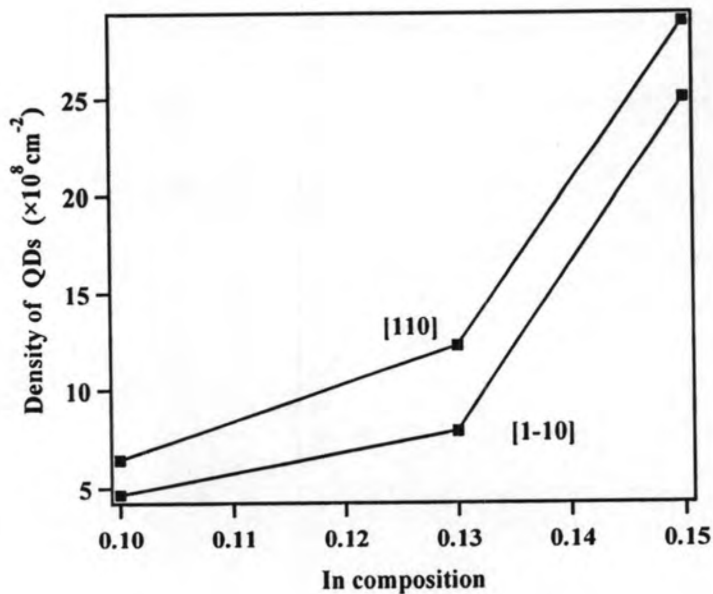

Figure 4.21 The density of QDs as a function of In composition.

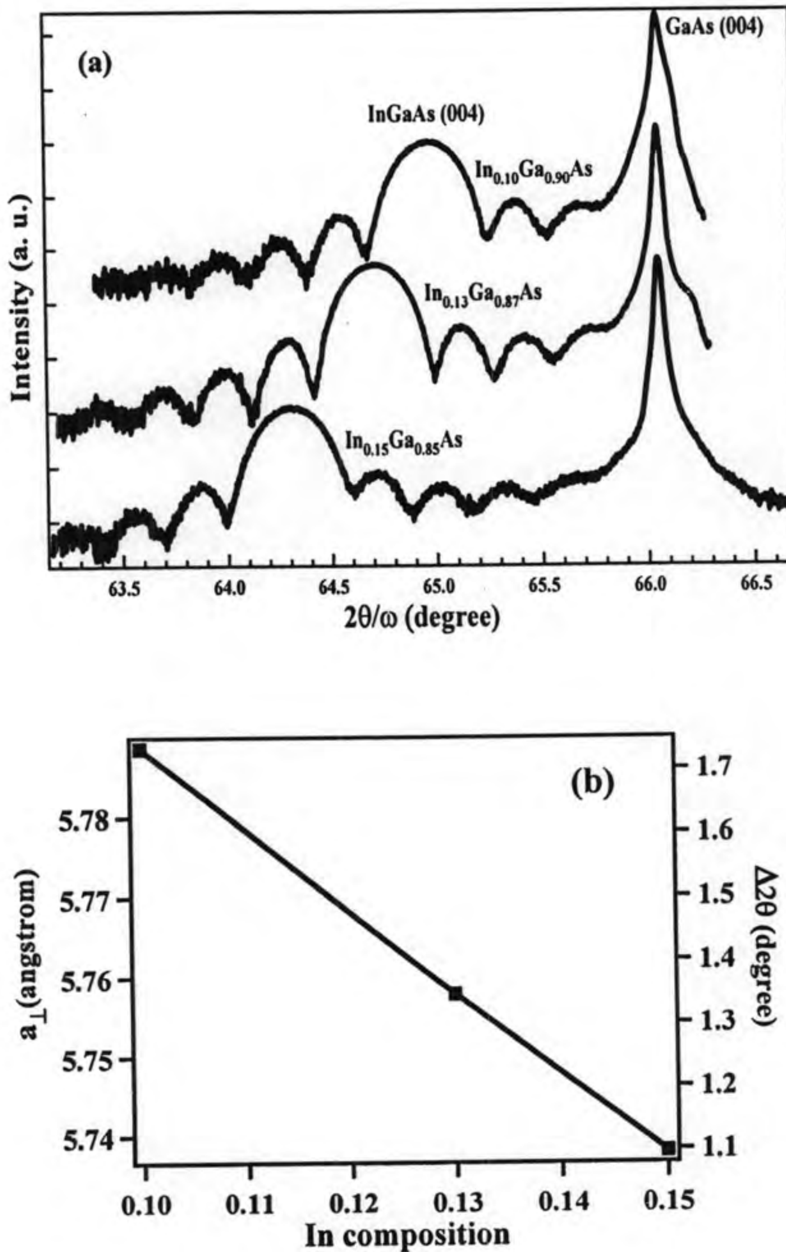

Figure 4.22 (a) HRXRD (004) $2\theta/\omega$ curves of InAs QDs grown on 50-nm InGaAs layer with various In composition of 0.10, 0.13 and 0.15 (b) the deduced lattice constants ($a_{\perp}$) of the three samples with 50-nm $In_xGa_{1-x}As$ layer (x=0.10, 0.13, and 0.15).

A similar result of increasing the diffraction angle of (004) InGaAs occurs as the In composition of the InGaAs layer is decreased. Figure 4.22(a) shows that (004) HRXRD spectra of the samples grown on 50 nm of $In_xGa_{1-x}As$ layers with various In

compositions (x=0.10, 0.13 and 0.15). Because of the distinct Pendellösung fringes observed in all samples in these figures, the InGaAs epitaxial layers in this sample are high quality. From the HRXRD results, the lattice constant in the growth direction ($a_{\perp}$) of InGaAs decreases as the In composition in the InGaAs layer increases is shown in Fig. 4.22(b). Therefore, the decrease in $a_{\perp}$ as an increasing of the In composition in InGaAs layer clearly reveals a higher degree of strain relaxation in InGaAs layer.

$In_xGa_{1-x}As/GaAs$ heteroepitaxial layers, having various compositions, have been analyzed using AFM and HRXRD techniques. The results have revealed that the strain in InGaAs layers is strongly dependent on the composition of InGaAs layers. The strain relaxation in InGaAs/GaAs layers increases as the thickness of InGaAs strained layers increases.

4.2.4 Effects of GaAs Capping Layers

Studies on capping process of conventional QDs grown on GaAs substrate with GaAs layers have been reported in literatures (Songmung et al., 2003; Suwaree, et al., 2005). However, no one has done the capping process of QDs grown on VS yet. Therefore, the effects of thin capping the QDs grown on InGaAs/GaAs cross-hatch VS with partial GaAs layers are investigated and reported in this section. In order to compare the capping process of QDs grown on between these two substrates, growth of QDs grown on GaAs substrate capped with thin GaAs layers are also repeated.

Figure 4.23 shows the AFM images of 1.8 ML of as grown self-assembled InAs QDs directly grown on a GaAs (001) substrate. The QDs are randomly distributed across the surface. The average QDs height is about 8 nm, the average diameter is about 50 nm, and the average dot density is $4.5\times10^{9}cm^{-2}$. Drastically collapsed QDs are found during the initial stage of capping process. When the QDs are capped with 9 ML of GaAs layer, the height of the QDs is reduced to less than 2 nm. The lattice mismatch between the InAs QDs and GaAs capping layer is about 7%. The lattice-mismatch capping layer increases the strain energy around the surface of the QDs and causes indium atoms detachment during the capping process. Therefore, a hole is left in the middle of the QD. The depth of the hole is about 0.632 nm and the width of the nanostructure becomes about 200 nm as shown by line scan result in Fig. 4.24.

Figure 4.23 AFM images of (a) as grown InAs QDs on GaAs substrate, (b) nano propeller structure created by capping the as grown QDs with 9 ML of GaAs layer and (c) regrown QDs on the nano propeller template.

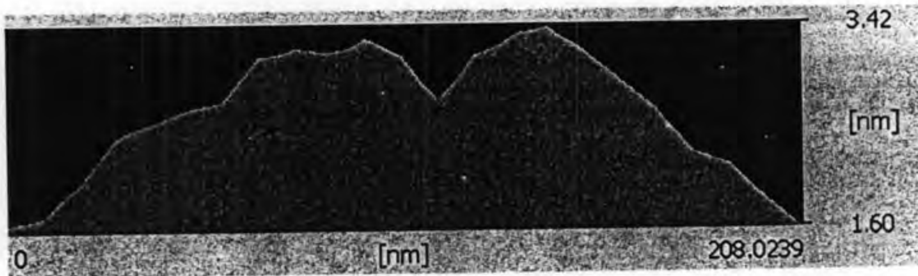

Figure 4.24 Line scan of InAs QDs capped partially with 9 ML of GaAs layer.

The nanostructure with the hole in the middle is named nano propeller because its shape (Suwaree et al., 2005). When QDs are regrown on the capping layer, QDs prefer to be deposited inside the hole where is the lowest energy sites for QDs. In all samples in Fig. 4.23, R_{GaAs} is 0.6 ML/s and R_{InAs} is 0.01 ML/s. The growth temperature of as grown QDs is 500°C and partial GaAs capping and regrowth of QDs are carried out at the T_{sub} 470°C. The thickness of InAs QDs regrown on the nanohole is required only 0.6 ML instead of 1.8 ML required for the QDs formation on the flat GaAs because nanoholes are easier nucleation sites than flat surfaces.

Even though the nanoholes can be seen in the middle the conventional QDs capped with partial GaAs layer, these are not seen in the middle of the QDs grown on VS which are capped partially with GaAs layer. Figures 4.25 and 4.26 show the 3×3 μm^2 AFM images and corresponding line scans of QD surface on 50 nm-

$In_{0.15}Ga_{0.85}As$ VS capped with partial GaAs layer. Line scans are taken along the [1-10] and [110] directions through the middle of the nanostructures. The shape of the QDs is drastically changed during capping with GaAs. Figure 4.25(a) is the reference InAs QDs with 30 sec GI time sample. The average dot and height of QDs for reference sample are 93 and 3.20 nm along [1-10] direction and 75 and 2.77 nm along [110] direction respectively.

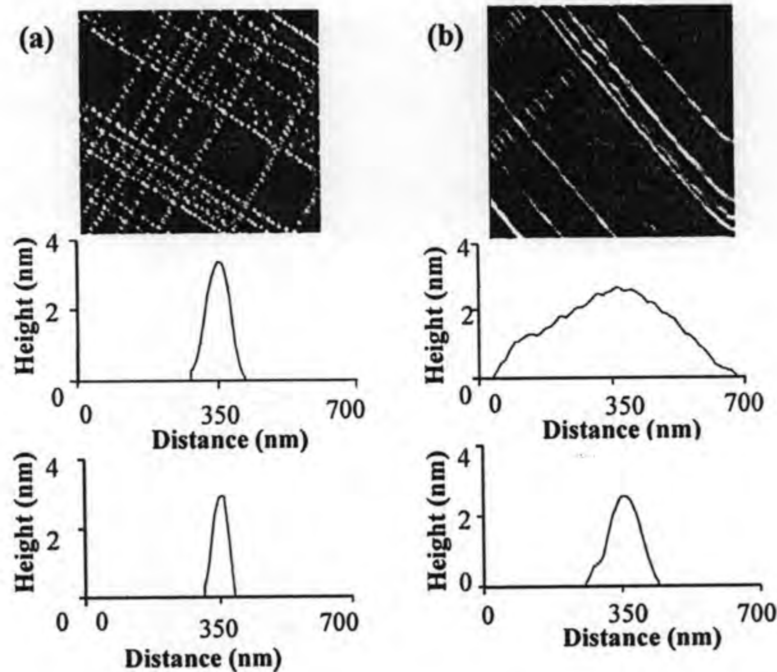

Figure 4.25 (a) 3×3 μm^2 AFM images of 0.8 ML of InAs QDs grown on 50-nm $In_{0.15}Ga_{0.85}As$/GaAs VS and capped partially with (b) 2 ML GaAs layers. The second rows and the third rows show the cross-sectional view of nanostructure for each corresponding AFM image along [1-10] and [110] directions.

Figure 4.25(b)-Fig. 4.26(b) shows the AFM images of collapsed nanostructures after reference sample is capped with GaAs. The capped QDs surface becomes flattering. Therefore these results are irreproducible to determine the shape of the QD and size during capping. The collapsed of the QDs and flattering phenomena have been explained by the chemical potential considerations (Srolovitz, 1989; Songmuang et al., 2003). The heights of QDs grown on flat GaAs substrate and cross-hatch VS are totally different. The height of as grown QDs (8 nm) on flat GaAs substrate is high enough to occur nanohole during capping process. In other words, the lattice

mismatch (strain) between the cap and the dot is high enough to drive In atoms away from the InAs QDs to the GaAs surface. On the other hand, the height of QDs on VS is less than 3 nm which is very small and the strain between the dot on VS and the cap is not high enough to move out In atoms from the QDs to GaAs surface. Songmuang et al. (2003) reported shape evolution of InAs QDs grown on GaAs (001) substrate by capping with various thicknesses of GaAs layer. Except the sample capped with 3 ML, all samples capped with 6, 15 and 30 ML are observed nanoholes in the middle of each QD. This group investigated the strain between the cap and dot by adjusting the In composition in InGaAs cap layer and found out that peak-to-valley depth of nanostructure becomes shallower and transforms into mountain structure when In composition is increased (strain is decreased). Therefore, the results of not observing nanoholes are attributed to the not high enough strain between the cap and the dot.

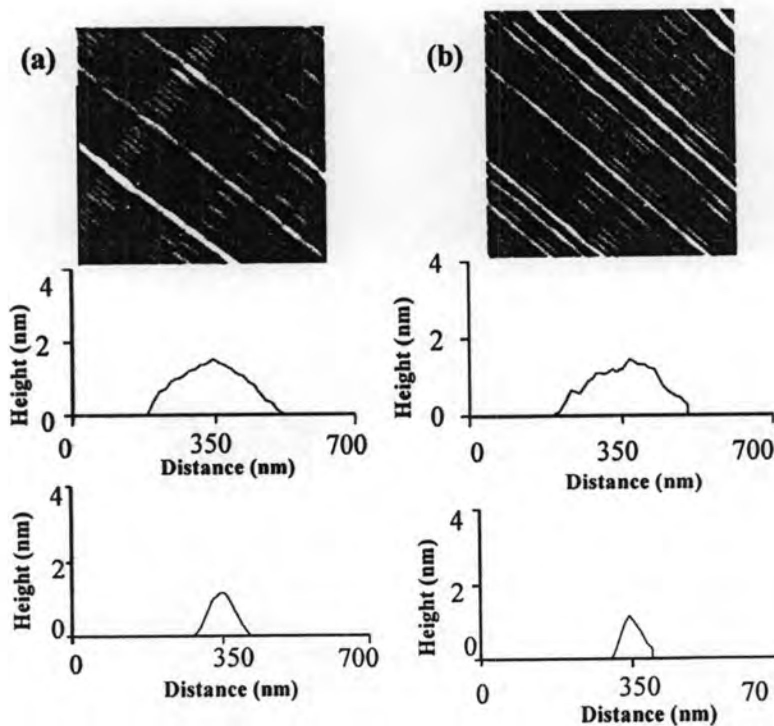

Figure 4.26 3×3 μm^2 AFM images of 0.8 ML of InAs QDs grown on 50-nm $In_{0.15}Ga_{0.85}As$/GaAs VS and capped partially with (a) 2 ML and (b) 6 ML GaAs layers. The second rows and the third rows show the cross-sectional view of nanostructure for each corresponding AFM image along [1-10] and [110] directions.

It is worthy to note that the QDs along <110> direction elongates towards the [1-10] direction only. This can be explained due to anisotropy diffusion of Ga adatoms in the [1-10] and [110] directions (Shiraishi, 1992). Therefore, the wings of each QD along [1-10] directions are overlapped with each other and become the nanostructure like QDs chain in this direction. Since the surface undulations of VS along [1-10] and [110] are different, the dimensions of QDs nucleated on VS are not the same. During the partial GaAs capping, the QDs along [1-10] directions are more prominent due to the increasing in length and decreasing in height of QDs in this direction. However, the QDs along the [110] directions are less prominent than before since the dimension of QDs along the [110] direction is smaller than [1-10] direction.

Figure 4.27 shows the AFM image of regrown InAs QDs on 50-nm $In_{0.15}Ga_{0.85}As$/GaAs cross-hatch VS capped partially with 6 ML of GaAs layer. The spotty patterns start to occur at 0.48 ML of InAs thickness. The QDs are seemed to be situated only along the [1-10] direction since the cross-hatch pattern along the [110] direction is less prominent during capping partially with GaAs layer.

Figure 4.27 AFM image of InAs regrown QDs on 50-nm $In_{0.15}Ga_{0.85}As$/GaAs cross-hatch VS capped partially with 6 ML of GaAs.

In conclusion, the structural properties of QDs grown on GaAs layer and cross-hatch VS have been investigated by partial capping GaAs layer process. The investigations show that large QDs grown on GaAs are developed into nanostructure with hole in the middle during the capping process. On the other hand, small QDs

grown on VS result in nanostructures with more prominent MDs along [1-10] direction and less prominent MDs along [110] directions during capping process. Consequently, the regrown QDs on these VS result in connected nanostructure along [1-10] direction.

Conclusion

This chapter concerns about the growth and characterization of InAs QDs grown on InGaAs/GaAs cross-hatch VS. InGaAs layers with thickness greater than the critical thickness are grown in order to get a cross-hatch pattern. The cross hatch patterns develop along the [1-10] and [110] directions. The average width and height along the [1-10] direction are 840 ± 230 nm and 1.06 ± 0.59 nm whereas those along the [110] direction are 505 ± 290 nm and 0.49 ± 0.34 nm, respectively which is attributed to strain asymmetries in dislocation densities. Thus, the hatches along the [1-10] direction are spaced further and are higher than those along the [110] direction.

After the formation of cross-hatch VS, InAs QDs are grown directly on the VS. A growth interruption (GI) time of 30 sec is introduced after the formation of QDs in order to improve the homogeneity of QDs. Statistical analyses of the AFM images indicate that the percentages of QDs formed on the cross hatches are 82%, 97% and 66% for samples with GI times of 0 sec, 30 sec and 60 sec, respectively.

In addition, the thickness and the In composition of the InGaAs layer are varied in order to vary the degree of strain relaxation and to form cross-hatch patterns with various morphologies. The strain relaxation in InGaAs increases with increasing In composition and thickness. QDs formed on the various thicknesses of strained layers show different alignment/grouping characteristics determined by the surface undulations of the underlying VS.

Finally, thin capping of QDs grown on GaAs substrate and on VS are comparatively studied in order to understand the morphological changes. At the same capping thickness, nanoholes are found in the middle of large QDs grown on GaAs layers but none are found in the middle of small QDs grown on cross-hatch VS. This is explained in terms of insufficient and asymmetry of strain energies in the underlying plane on which QDs are grown.